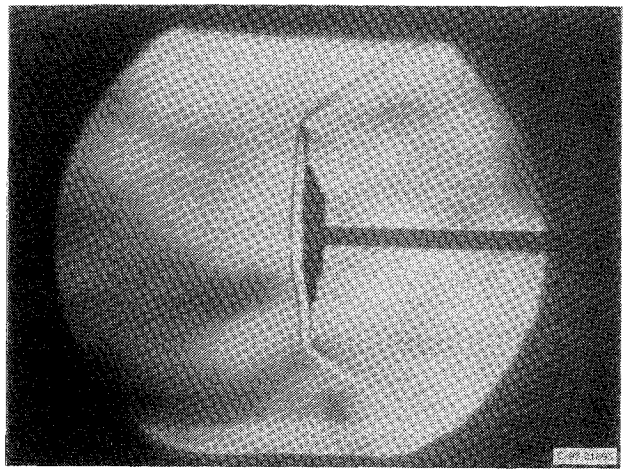

Fig. 4 Schlieren pictures of dummy (no electronics) drag probes (Mach 2).

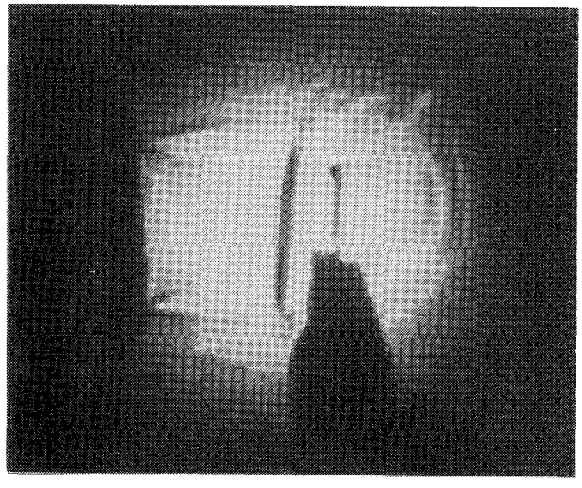

Fig. 5 Laser shadowgraphs of drag probe (Mach 2).

probe and the freestream velocity head. In fact, the results from the two sets of tests demonstrate that it is not necessary to calibrate the drag probe in a supersonic flow; subsonic calibration is sufficient. To test whether the extrapolation of the subsonic calibration into the supersonic regime derived before was valid, we tested the probe in a small jet facility that was capable of both subsonic and supersonic flows. The velocity head calculated from the other sensors' data (room and line pressures and room temperature), was plotted. Equation (2) was also plotted and is seen to be very accurate, showing that the subsonic calibration of the drag probe is adequate. The standard deviation between the two calibrations is 0.5813.

Dummy drag probes were also tested in the 5 × 5 in. (12.7 × 12.7 cm) supersonic facility to obtain schlieren images of the shock structure around the drag probe. The image shown in Fig. 4 seems to support the assumption that the shock in front of the drag probe is indeed a normal shock. The laser shadowgraphs from the combined subsonic and supersonic tests confirm a normal shock as well.

The differences between Figs. 4 and 5 with respect to the shock shape located away from the center of the probe element (the beam) as seen in the laser shadowgraphs and in the schlieren photographs are largely due to the jet from the small 1-in. nozzle vs the core flow in the larger 5 × 5 in. (12.7 × 12.7 cm) test section. The velocity profile of the jet was still tracing out a parabolic shape with the small nozzle, whereas the velocity profile in the larger test section was largely flat in the core where the probes were placed. This difference does not affect the results because the small probe element is mostly covered by the normal shock, as Figs. 4 and 5 show.

V. Conclusions

The drag-force anemometer, or drag probe, can be most useful in supersonic- as well as subsonic-flow regimes. Furthermore, a normal-shock relation between the subsonic and supersonic drag-probe results has been established. This relation indicates that a subsonically calibrated drag probe is supersonically calibrated as well.

References

[1]Cole, G. L., and Richard, J. C., "Supersonic Propulsion Simulation by Incorporating Component Models in the LArge Perturbation INlet (LAPIN) Computer Code," NASA TM 105193, Dec. 1991.

[2]Krause, L. N., and Fralick, G. C., "Miniature Drag-Force Anemometer," NASA TM Rept. X-3507, June 1977.

[3]Krause, L. N., and Fralick, G. C., "Miniature Drag-Force Anemometers," *Instrument Society of America Transactions*, Vol. 21, No. 1, 1982, pp. 117–130.

[4]Fralick, G. C., "Extending the Frequency of Response of Lightly Damped Second Order Systems: Application to the Drag Force Anemometer," NASA TM 82927, Aug. 1982.

[5]Krause, L. N., and Fralick, G. C., "Some Dynamic and Time-Averaged Flow Measurements in a Turbine Rig," *Journal of Engineering for Power*, Vol. 102, No. 1, 1980, pp. 223, 224.

[6]Hoerner, S. F., *Fluid Dynamic Drag; Practical Information on Aerodynamic Drag and Hydrodynamic Resistance*, 1965, pp. 3–14 (published by the author).

[7]Ames Research Staff, "Equations, Tables and Charts for Compressible Flow," NACA Rept. 1135, NASA Ames–Dryden Flight Research, 1953.

[8]Gettelman, C. G., and Krause, L. N., "Characteristics of a Wedge with Various Holder Configurations for Static Pressure Measurements in Subsonic Gas Streams," NACA RM E51G09, Sept. 1951

Mass Spectrometer Measurements of Test Gas Composition in a Shock Tunnel

K. A. Skinner* and R. J. Stalker†
University of Queensland,
Brisbane 4072, Queensland, Australia

Introduction

SHOCK tunnels afford a means of generating hypersonic flow at high stagnation enthalpies, but they have the disadvantage that thermochemical effects make the composition of the test flow different to that of ambient air. The composition can be predicted by numerical calculations of the nozzle flow expansion, using simplified thermochemical models, and in the absence of experimental measurements, it has been necessary to accept the results given by these calculations.

This Note reports measurements of test gas composition, at stagnation enthalpies up to 12.5 $MJkg^{-1}$, taken with a time-of-flight mass spectrometer. Limited results have been obtained in previous measurements.[1] These were taken at higher stagnation enthalpies and used a quadruple mass spectrometer. The time-of-flight method was preferred here because it enabled a number of complete mass spectra to be obtained in each test, and because it gives good mass resolution over the range of interest with air (up to 50 amu).

Experiments

The experiments were conducted in the free piston shock tunnel T4 at the University of Queensland,[2] using a helium-argon mixture as driver gas. The shock tube, of 10-m length and 75-mm diam, was operated in the shock-reflected mode and supplied shock-heated air to a contoured hypersonic nozzle with a throat diameter of 25.4 mm and an exit diameter of 261 mm. As shown in Fig. 1a, the mass

Received Feb. 24, 1995; revision received June 16, 1995; accepted for publication July 6, 1995.

*Postgraduate Student, Department of Mechanical Engineering.

†Emeritus Professor of Space Engineering, Department of Mechanical Engineering. Associate Fellow AIAA.

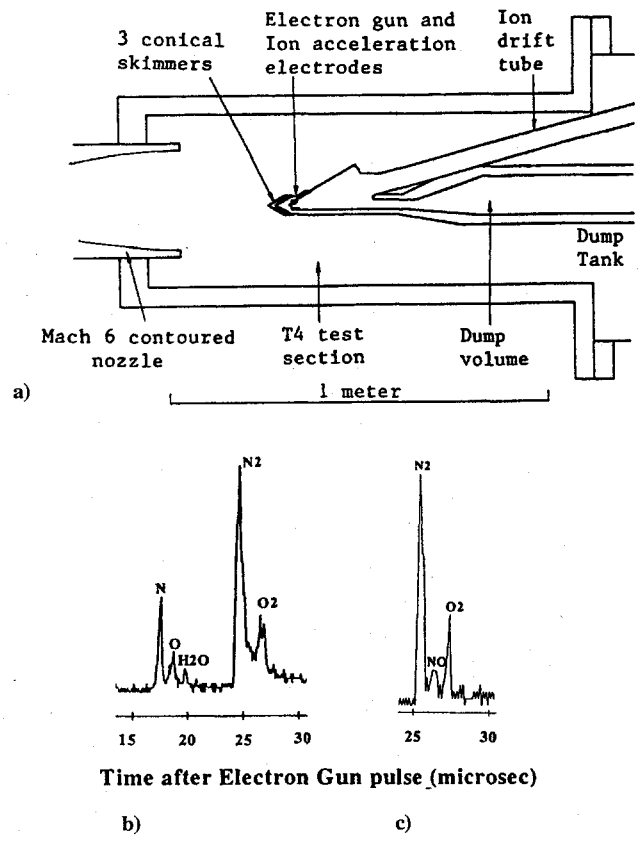

Fig. 1 Mass spectrometer: a) experimental arrangement, b) typical mass spectrum, and c) improved resolution mass spectrum.

spectrometer sampled the flow from a point on the nozzle centerline, well within the test cone of the nozzle flowfield.

The stagnation enthalpy was calculated for equilibrium air from the shock speed and initial shock tube filling pressure, with an isentropic expansion to the measured nozzle reservoir pressure of 14.0 ±2.5 MPa. The estimated accuracy of the stagnation enthalpy was from +4 to −8%. To avoid problems with driver gas contamination of the test flow, the test time was confined to a period from 0.5 to 1.0 ms after initiation of flow in the test section, and the stagnation enthalpy was limited to 12.5 $MJkg^{-1}$.

The mass spectrometer is described in Ref. 3. Essentially, it sampled the flow through a series of three conical skimmers to form a molecular beam. This was bombarded by a 250-eV electron beam for 200 ns every 55 μs, and each time a pulse of ions was produced that passed into the 1-m-long drift tube, and hence to an electron multiplier detector at the end of the tube. Since the time of arrival of the ions depended on their mass, a mass spectrum of the type shown in Figs. 1b and 1c was obtained every 55 μs and was recorded by a 50-MHz digital oscilloscope.

Peaks of N_2, O_2, N, and O are evident in the spectrum of Fig. 1b, as well as some residual H_2O. The area under each peak is proportional to the number of particles of that particular mass to reach the detector. There is clearly a problem with overlap of the peaks of N_2, NO, and O_2, and this particularly affects measurement of the NO peaks. Therefore some tests were made in which fewer spectra were taken, but the sampling rate of the oscilloscope was increased. The resolution was therefore improved, as shown in Fig. 1c, and these spectra were used for measurements of the NO peak.

Results and Discussion

The ratio of the measurements of peak sizes is presented in Fig. 2 for O_2/N_2, NO/N_2, and O/O_2. Each of the points plotted is the mean of a number of readings during a test and therefore may be regarded as the mean of a statistical sample. The error bars indicate the standard deviation of that mean.

The measurements are compared with theoretical curves for the relative peak sizes. These were obtained by first performing

Table 1 Electron impact ionization cross sections at 250 eV

Process	Cross section, cm^2	Error, %	Reference
$O_2 + e \rightarrow O_2^+ + 2e$	1.57×10^{-16}	13	5
$O + e \rightarrow O^+ + 2e$	1.08×10^{-16}	5	6
$N_2 + e \rightarrow N_2^+ + 2e$	1.68×10^{-16}	8	7
$NO + e \rightarrow NO^+ + 2e$	1.89×10^{-16}	20	8

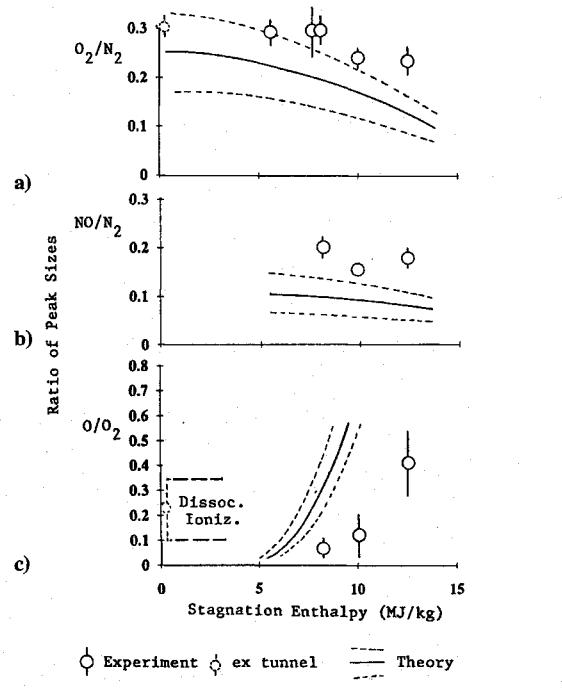

Fig. 2 Relative size of mass peaks: a) molecular oxygen vs molecular nitrogen, b) nitric oxide vs molecular nitrogen, and c) atomic oxygen vs molecular oxygen.

numerical calculations[4] of the inviscid nonequilibrium steady expansion through the shock tunnel nozzle to yield the freestream species concentrations. These were then used to obtain values for the relative size of the mass spectra peaks. The effect of mass separation in the molecular beam was assessed by testing in the shock tunnel with known mixtures of nitrogen and helium, and nitrogen and argon. This indicated that the relative enhancement of the molecular species considered was less than 10%. The relative number of ions produced was determined from the ionization cross sections given in Table 1, and the relative efficiency with which ions were collected was taken as unity. This was checked by operating the instrument ex tunnel (i.e., outside the shock tunnel), with the first of the three skimmers replaced by a solenoid valve, which delivered a short pulse of room air to the mass spectrometer. The measured ratio of the O_2 peak area to N_2 peak area was 0.30 ±0.02, which, allowing for the uncertainty in ionization cross sections, compared satisfactorily with the expected value of 0.25.

To calculate theoretical values for the peaks of atomic oxygen, the combined effect of mass separation and ion collection efficiency was obtained from the helium/nitrogen and nitrogen/argon results by assuming that these effects varied linearly with the mass ratio of the two species, yielding a factor of 2.0 ±0.4 for enhancement of O with respect to O_2. This was applied to the predicted numerical values for relative concentrations of O and O_2, and taking into account the ionization cross sections, the theoretical curve in Fig. 2c was obtained. Because of uncertainties in mass separation and ion collection efficiencies, as well as in ionization cross sections, a possible error attaches to all of the theoretical curves. The limits of this are indicated by the broken lines on either side of each curve.

Note that the effect of dissociative ionization of the O_2 molecule in the mass spectrometer, with production of ionized O atoms, has not been taken into account in obtaining the theoretical curve of Fig. 2c. This is because the experimental results in the tunnel show

the ratio of peak sizes increasing with enthalpy from a value near zero, and this is not consistent with the presence of a substantial number of O ions due to dissociative ionization. On the other hand, it must be observed that results of the ex tunnel tests shown in Fig. 2c demonstrate that substantial dissociative ionization does indeed take place in air that is supplied from a room temperature source. It may be speculated that this difference is due to thermal excitation of the O_2 molecules in the tunnel flow, leading to an increased velocity spread and consequent lowered collection efficiency of the O ions resulting from dissociative ionization. However, until this apparent anomaly is resolved, some doubt must be attached to the experimental results of Fig. 2c. Therefore, notwithstanding the remark made later concerning their validity, their worth is mainly in indicating the stagnation enthalpy at which the rise in O atom concentration due to freestream dissociation takes place.

The overall ratio of the number of atoms of oxygen in any form to nitrogen in any form can be obtained from the results in Fig. 2. If the ex tunnel result in Fig. 2a is used to generate a calibration factor for the O_2/N_2 ratio, values of 0.33 $\pm$0.04, 0.27 $\pm$0.03, and 0.30 $\pm$0.04 are obtained for the overall ratio at stagnation enthalpies of 8.3, 10, and 12.5 MJ kg^{-1}, respectively. The expected value is 0.27 $\pm$0.05, the quoted error limits resulting from residual uncertainties in the ionization cross sections, together with the mass separation and ion collection efficiencies, after the calibration for the O_2/N_2 ratio has been taken into account. Thus, the values for the overall oxygen/nitrogen ratio fall within the quoted limits of error and provide confirmation of the experimental measurements.

It is worth remarking that, at 12.5 $MJkg^{-1}$, the measured O/O_2 value in Fig. 2c contributes a substantial 0.08 of the total oxygen/nitrogen ratio of 0.30, thereby providing an indirect confirmation of the O/O_2 measurement.

It can be seen that the experimental measurements in Fig. 2 generally fall outside the theoretical limits indicated by the broken lines. In Fig. 2a the proportion of molecular oxygen exceeds theoretical limits as the stagnation enthalpy is increased. This is consistent with the results in Fig. 2c, which shows the proportion of atomic oxygen remaining at low levels for much higher enthalpies than predicted. The proportion of nitric oxide is shown in Fig. 2b and is seen to be in excess of predicted values, at least for the range of stagnation enthalpies covered by the results. The numerical model[4] on which the theoretical curves are based gives freestream compositions that are consistent with those given by other numerical models.[9] Therefore, even when allowance is made for the experimental uncertainties, there are clear discrepancies between the theory of nonequilibrium nozzle flow and the results of these experiments, indicating a need for further experimental and theoretical work. Until these discrepancies are resolved, predictions of the composition of test section flows in high enthalpy facilities should be treated with caution.

Acknowledgments

The authors gratefully acknowledge the support received from the Australian Research Council and through NASA Grant NAGW-674.

References

[1]Crane, K. C. A., and Stalker, R. J., "Mass-Spectrometric Analysis of Hypersonic Flows," *Journal of Physics D: Applied Physics*, Vol. 10, 1977, pp. 679–695.

[2]Stalker, R. J., "Recent Developments with Free Piston Drivers," *Proceedings of the 17th International Symposium on Shock Waves & Shock Tubes*, American Inst. of Physics, AIP Conf. Proceedings 208, New York, 1990, pp. 96–105.

[3]Skinner, K. A., and Stalker, R. J., "A Time-of-Flight Mass Spectrometer for Impulse Facilities," *AIAA Journal*, Vol. 32, No. 11, 1994, pp. 2325–2328.

[4]Lordi, J. A., Mates, R. E., and Moselle, J. R., "Computer Program for the Numerical Solution of Non-Equilibrium Expansions of Reacting Gas Mixtures," NASA CR-472, May 1966.

[5]Krishnakumar, E., and Srivastava, S. K., "Cross-Sections for Electron Impact Ionization of O_2," *International Journal of Mass Spectrometry and Ion Processes*, Vol. 113, 1992, pp. 1–12.

[6]Bell, K. L., Gilbody, H. B., Hughes, J. G., Kingston, A. E., and Smith, F. J., "Recommended Data on the Electron Impact Ionization of Light Atoms and Ions," *Journal of Physical and Chemical Reference Data*, Vol. 12, 1983, pp. 891–916.

[7]Krisnakumar, E., and Srivastava, S. K., "Cross-Sections for the Production of N_2^+, N^+, N_2^{2+} and N_2 by Electron Impact on N_2," *Journal of Physics B: Atomic and Molecular Physics*, Vol. 23, 1990, pp. 1893–1903.

[8]Rapp, D., and Englander-Golden, P., "Total Cross-Sections for Ionization and Attachment in Gases by Electron Impact. I. Positive Ionization," *Journal of Chemical Physics.*, Vol. 43, 1965, pp. 1464–1479.

[9]Sagnier, P., and Marraffa, L., "Parametric Study of Thermal and Chemical Nonequilibrium Nozzle Flow," *AIAA Journal*, Vol. 29, No. 3, 1991, pp. 334–343.

Calibration of Preston Tubes

Dietrich W. Bechert*
DLR, German Aerospace Research Establishment, Berlin 10623, Germany

Introduction

IN this Note, a simple equation is provided that relates Preston tube pressure output and wall shear stress. The Preston tube technique[1–6] probably is the most convenient method to measure turbulent skin friction. The classical arrangement consists of a pitot tube mounted onto a wall surface. In addition, a hole in the wall in the vicinity is required to measure the static pressure; see Fig. 1. The pressure difference between pitot tube and static pressure hole represents the output Δp of the probe. In some applications,[3] the static pressure is collected by a second tube with one or more holes on its side. This arrangement permits the dual probe to move easily on a given surface. Albeit inferior in its precision to, e.g., floating element balances, a Preston tube produces an accuracy of about 5% or better,[5] which is perfectly satisfactory in many applications. One such application is the determination of the surface shear stress on a wind-tunnel model to select the proper riblet spacing of a drag-reducing riblet film.

Calibration

A general calibration curve relating the output Δp to the wall shear stress τ has been compiled by Rechenberg[3,4]; see Fig. 1. The quantities in this plot are nondimensionalized as follows:

$$\Delta p^+ = \Delta p d^2/\rho\nu^2; \qquad \tau^+ = \tau d^2/\rho\nu^2 \tag{1}$$

where d is the diameter of the probe, and ρ and ν are density and kinematic viscosity of the fluid. The only disadvantage of the data in Fig. 1 is that they are not available in the form of a simple equation being valid over the whole parameter range. Asymptotic equations have been derived for the upper parameter regime, assuming either a logarithmic or a $\frac{1}{7}$ power law for the mean flow distribution. For the latter, the result turns out to be very simple:

$$\tau^+ = \frac{(\Delta p^+)^{\frac{7}{8}}}{19.72} \tag{2}$$

Close to the wall, at low Δp^+ and τ^+, however, the probe is immersed in the Couette-type flow regime of the viscous sublayer, and there Eq. (2) is not valid anymore. With the same momentum considerations as the ones used by Rechenberg[4] to derive Eq. (2), we find for a Couette flow impinging on the probe with circular cross section

$$\tau^+ = 4\sqrt{\Delta p^+/3} \tag{3}$$

Besides fitting the data at low Δp^+ in Fig. 1, this equation also permits the use of Preston tubes in laminar flows. As in turbulent flows, however, the probe size must be significantly smaller than the

Received May 8, 1995; revision received July 11, 1995; accepted for publication July 11, 1995.

*Senior Scientist, Abt. Turbulenzforschung, Müller-Breslau-Str. 8. Senior Member AIAA.